31st Annual International Conference of the IEEE EMBS
Minneapolis, Minnesota, USA, September 2-6, 2009

Estimating vascular volume fraction in a network of small blood vessels with high-frequency power Doppler ultrasound

Stephen Z. Pinter, *Student Member, IEEE,* and James C. Lacefield, *Member, IEEE*

***Abstract*— Quantitative images of high-frequency (> 20 MHz) power Doppler ultrasound can be difficult to obtain in the presence of flow artifacts due to power Doppler's sensitivity to operator-dependent acquisition settings. To improve flow quantification, color pixel density (CPD) can be plotted as a function of wall filter cut-off velocity to produce a wall-filter selection curve that can be used to estimate vascular volume fraction by locating the plateau along the curve. The behavior of the wall-filter selection curve in a multiple-vessel region of interest is studied using a custom-designed multiple-vessel flow phantom. The flow phantom is capable of mimicking a range of blood vessel sizes (200–300 μm), blood flow velocities (1–10 mm/s), and blood vessel orientations (long-axis and transverse). At high flow rates, single-vessel wall-filter selection curves superimpose to produce a multiple-vessel curve where the CPD at the left-most plateau corresponds with the actual vascular volume fraction. However, interpretation of the multiple-vessel wall-filter selection curve is not straightforward when the flow rate in the vascular network is low.**

I. INTRODUCTION

High-frequency power Doppler ultrasound's sensitivity to blood flow in small vessels is particularly useful when studying physiological and pathological angiogenesis in small-animal models [1]. Imaging these angiogenic models can be challenging due to the complex spatial and temporal distributions and slow flow velocities of small blood vessels [2], [3]. Obtaining a quantitative power Doppler image in such environments can be complicated by color pixel artifacts, the presence of which depends on factors such as spectral broadening, motion clutter, dwell time, noise, and acquisition settings such as the wall filter cut-off velocity.

In the presence of substantial Doppler artifacts, color pixel density (CPD) and related vascularity metrics will not provide accurate estimates of the true vascular volume fraction. For example, in preclinical studies of cancer-associated angiogenesis [4], [5], [6], investigators typically quantify blood flow using longitudinal measurements of CPD. Angiogenic vasculature may undergo significant changes in structure and function during tumor progression or treatment. If, for example, an investigator fixes the wall filter cut-off velocity, the system will fail to detect any biological changes from vessels with flow velocities below that cut-off. An improved approach might involve adapting the instrument settings at each imaging time point to ensure detection of as much of the true angiogenic vasculature as possible while minimizing Doppler artifacts. Such an approach requires an objective method for selecting scanner settings.

Computation of normalized fractional moving blood volume is a well-known approach for improving flow quantification with power Doppler ultrasound [7], [8]. Normalized fractional moving blood volume compensates for depth and attenuation; however, power Doppler images are also influenced by operator-dependent acquisition settings. These settings can affect the balance between true- and false-positive flow fractions, and therefore a normalization applied in the presence of artifacts will normalize, but not eliminate, those artifacts.

In a previous study [9], we developed a wall-filter selection curve method to identify a wall filter cut-off velocity that yielded the CPD value that was the best estimate of vascular volume fraction for a region of interest (ROI). That study demonstrated that the wall filter cut-off velocity resulting in the best-estimate CPD corresponded with the location of a characteristic plateau in the curve. The best choice of wall filter cut-off velocity varied depending on the flow conditions in the region under investigation. That study was limited to idealized cases in which the ROI contained a long-axis view of a single vessel.

In this paper, the wall-filter selection curve is studied in a multiple-vessel scenario that challenges the method with a more realistic environment where vessels with a range of flow velocities and diameters are present in both long-axis and transverse configurations. A custom-made multiple-vessel flow phantom was developed that mimicked vessel configurations observed in a transgenic mouse prostate cancer model [5]. The flow phantom is used to study the relationship between true- and false-positive color pixel fractions and CPD as the wall filter cut-off velocity is varied. The experimental data demonstrate the conditions required for a plateau to exist and give an accurate and reliable estimate of the actual vascular volume fraction in a multiple-vessel ROI.

II. MATERIALS AND METHODS

A. Four-vessel Flow Phantom

Experiments were performed with a wall-less flow phantom constructed using four polymer tubes (Paradigm Optics, Vancouver, WA, USA) composed of either acrylic (polymethyl methacrylate) or polyethylene terephtalate glycol (PETG) to form flow channels with outer diameters of 200, 250, 250, and 300 μm. The polymer tubing was connected to a 26-G needle hub from which the steel needle tip had been

S. Z. Pinter is with the Biomedical Engineering Graduate Program and Robarts Research Institute, University of Western Ontario, London, Ontario, Canada. spinter@ieee.org

J. C. Lacefield is with the Biomedical Engineering Graduate Program, Departments of Electrical and Computer Engineering and Medical Biophysics, and Robarts Research Institute, University of Western Ontario, London, Ontario, Canada. jlacefield@eng.uwo.ca

978-1-4244-3296-7/09/$25.00 ©2009 IEEE

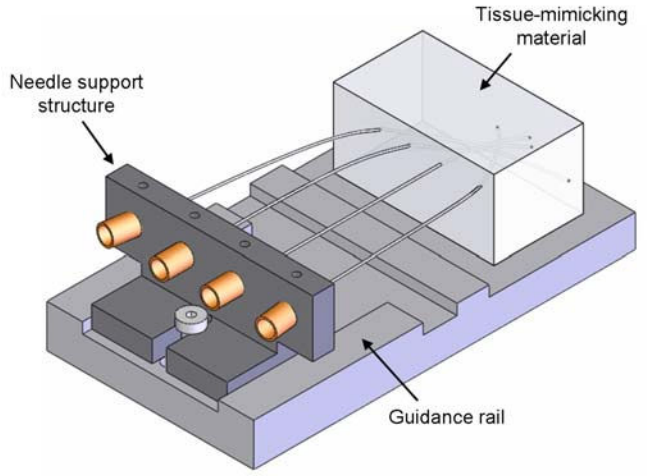

Fig. 1. Isometric view of the four-vessel flow-phantom support structure showing the base (dark grey), needle support structure (black), needles (orange), and gelatin mold (light grey). The size of the microtubing and vessel cavity have been exaggerated for display purposes.

removed so that blood-mimicking fluid could pass directly through the needle hub into the tubing.

In all experiments, the four needle/tubing combinations were held securely in the needle support structure shown in Fig. 1. All four microtubes were guided inside the mold to appear within the same 2.5×3-mm^2 ROI but with different orientations. For example, one vessel may pass through the ROI longitudinally, whereas another may pass through transversely. Vessel configurations were determined based on microfil-enhanced micro-CT images of tumor vascularity in a transgenic mouse prostate cancer model [5].

After the four vessels were positioned inside the hollow form in Fig. 1, a tissue-mimicking gelatin mixture (similar to [10]) was poured inside the form to surround the tubing. Once the gelatin mixture solidified, the tubing was partially retracted by sliding the needle support back along its guidance rails. All four vessel cavities were then infused with blood-mimicking fluid from a single 10-cc syringe controlled using a syringe pump (NE-1000 Syringe Pump, New Era Pump Systems Inc., Wantagh, NY, USA). Blood-mimicking fluid was made following the technique developed by Ramnarine *et al.* [11]. The blood-mimicking fluid consisted of 5-μm average diameter nylon scatterers with a volume concentration of 2%.

Blood-mimicking fluid was injected by the 10-cc syringe into a one-to-four flow distribution network that distributed fluid into the four vessel cavities. One-way polycarbonate stopcocks (#30600-01, Cole-Parmer Canada Inc., Montreal, QC, Canada) were inserted between the output of the flow distribution network and the needle/tubing combination, which enabled perfusion of each vessel individually or all vessels simultaneously.

B. Image Acquisition

Power Doppler images were acquired using a Vevo 770 swept-scan high-frequency ultrasound system (VisualSonics, Toronto, ON, Canada) with a 30-MHz transducer (RMV707, 12.7 mm focal length, 55 μm axial resolution, 115 μm lateral resolution, 2.2 mm depth of field). The transducer was positioned so that the focus was 4.5 mm below the surface of the tissue phantom. The Doppler ROI included 1.25 mm above and below the focus and had a lateral width of approximately 3 mm. The following acquisition settings were used in all experiments: 9×9 mm^2 field of view, 100% transmit power, 2 cycle pulse length, 20 dB receiver gain, 2 kHz pulse repetition frequency, and 0.5 mm/s scan speed. The auto-histogram feature was used to set the minimum value of the display dynamic range to just above the noise floor as described in [9].

TABLE I
SYRINGE PUMP FLOW RATES AND CORRESPONDING INDIVIDUAL VESSEL FLOW VELOCITIES

Pump flow rate (μL/h)	Vessel diameter (μm)	Flow velocity (mm/s)
1500	200	1.35
	250	2.1
	300	2.4
3000	200	2.7
	250	4.2
	300	4.8
6000	200	5.4
	250	8.4
	300	9.6

Three syringe pump flow rates were tested for each four-vessel configuration (Fig. 2): 1500, 3000, and 6000 μL/h. Table I shows the calculated individual vessel flow velocities for each of the syringe pump flow rates. Five different flow states were evaluated for each four-vessel configuration by adjusting the stopcocks: each of the four vessels was perfused individually and then all vessels were perfused simultaneously by opening all valves.

Power Doppler and B-mode cine loops (15 and 200 frames, respectively) were recorded at multiple wall filter cut-off velocities for each combination of flow state and four-vessel configuration. The wall filter cut-off velocity was increased from a minimum value of 0.3 mm/s in increments of 0.2 mm/s for the 3000- and 6000-μL/h flow rates, and in increments of 0.1 mm/s for the 1500-μL/h flow rate. The wall filter cut-off velocity was increased until minimal color pixels were present in the power Doppler image.

C. Image Analysis

Vessel segmentation was performed by first subtracting two B-mode frames to enhance the contrast between the vessel(s) and tissue and then manually segmenting the subtracted image in Adobe Photoshop CS2 (Adobe Systems Inc., San Jose, CA, USA). The resulting vessel boundaries were superimposed onto the power Doppler image. True- and false-positive color pixel fractions were computed in the 2.5×3-mm^2 ROI using an algorithm implemented in Matlab 7 (The MathWorks Inc., Natick, MA).

Wall-filter selection curves were constructed for each combination of flow state, four-vessel configuration, and syringe

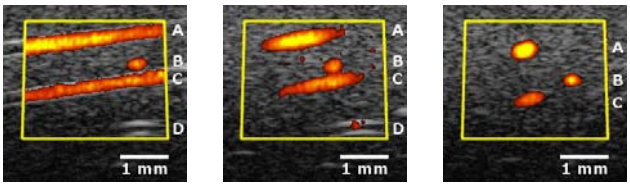

(a) High vascularity (b) Medium vasc. (c) Low vascularity

Fig. 2. Power Doppler images acquired with the 6000-μL/h flow rate and 0.9-mm/s wall filter cut-off velocity for vessel configurations designed from micro-CT images of tumor vascularity. The three vessel configurations are representative of (a) high, (b) medium, and (c) low vascularity. Individual vessels are referred to by the letters A–D, as indicated on each configuration. Vessel A is a 300-μm diameter vessel, vessel B is a 200-μm diameter vessel, and vessels C and D are 250-μm diameter vessels. The yellow box is the region of interest, which is centered axially at the focal distance.

pump flow rate. Data points for these wall-filter selection curves were computed over 11 power Doppler frames and the average value plotted with a 95% confidence interval.

Wall-filter selection curves showed a characteristic plateau at intermediate cut-off velocities. The presence and extent of this plateau was quantified using a metric that computed relative change in CPD, $|\Delta CPD|/CPD$, [9]. The length of the plateau was quantified by identifying the range of wall filter cut-off velocities that produce $|\Delta CPD|/CPD$ values below an empirically determined threshold of 0.14 that are bounded by $|\Delta CPD|/CPD$ values greater than 0.14.

III. RESULTS AND DISCUSSION

A. Flow Phantom Wall-filter Selection Curves

Figure 3 shows wall-filter selection curves acquired for the high vascularity (Fig. 2(a)) ROI while perfusing all vessels simultaneously and infusing at the 6000- and 3000-μL/h flow rates. Similar to the form of Fig. 3(b), the single-vessel wall-filter selection curves for vessels A–D (not shown) showed that the plateau divides the curve into three regions: (1) an overestimation of the vascular volume fraction to the left of the plateau, (2) an underestimation to the right of the plateau, and (3) a region at intermediate cut-off velocities where CPD is approximately equal to the actual vascular volume fraction.

Figure 3(a) shows that two gradually decreasing plateaus are present when all vessels are perfused simultaneously at a flow rate of 6000 μL/h. The left-most gradually decreasing plateau approaches the actual total vascular volume fraction in the ROI, while the second plateau approaches the actual vascular volume fraction of vessel A only.

In the above scenario, it was straightforward to estimate the actual total vascular volume fraction by identifying the CPD estimate corresponding with the left-most plateau. However, in other cases the left-most plateau for a multiple-vessel ROI may not coincide with the total vascular volume fraction. Figure 3(b) shows that only a single plateau is present when the flow rate is decreased to 3000 μL/h. For this lower flow rate, the plateau approaches the vascular volume fraction of vessel A only (dashed-dotted line) rather than the vascular volume fraction of all vessels (dashed line). This occurs because the detectability of vessels B–D is substantially reduced in the wall filter cut-off range

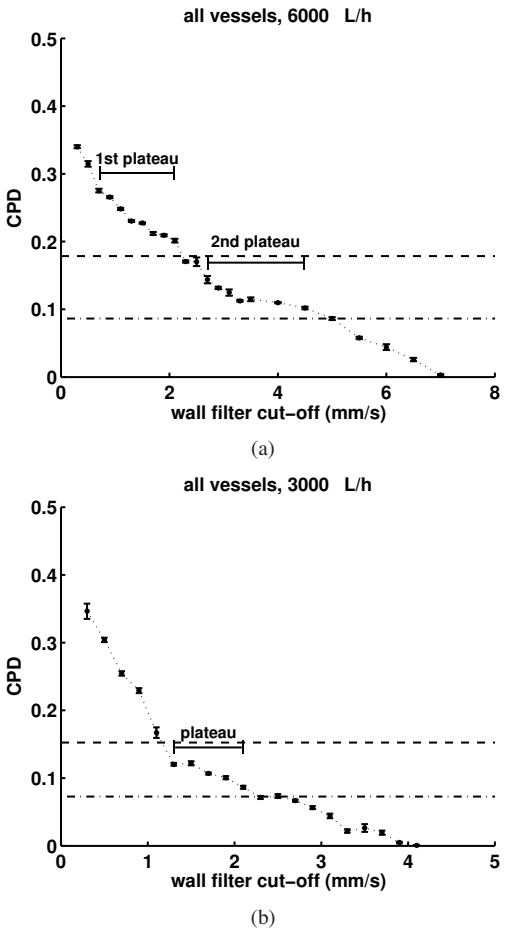

Fig. 3. Flow-phantom wall-filter selection curves acquired while infusing the region of interest (ROI) representative of high vascularity at the (a) 6000- and (b) 3000-μL/h flow rate. Error bars indicate 95% confidence intervals for an 11-frame data set. Dashed lines indicate the actual vascular volume fraction computed in the 2.5×3-mm^2 ROI defined in Fig. 2(a). Dashed-dotted lines indicate the actual vascular volume fraction of vessel A only.

1.0–1.5 mm/s. Once these three lower-velocity vessels are absent from the power Doppler image, the vessel with the highest flow velocity, vessel A, becomes the primary source of color pixels until a cut-off of 2.1 mm/s, at which point the CPD is 0.0864 (the actual vascular volume fraction of vessel A is 0.0727).

B. Estimated and actual vascular volume fractions

Figure 4 shows comparisons between the measured CPD and actual vascular volume fraction for all combinations of flow state, syringe pump flow rate, and vessel configuration. Common among all three vessel configurations with the 3000-μL/h flow rate is the observation that when vessel C, and in some cases vessels B or D, produces a short ($<$ 0.5 mm/s) plateau, the measured CPD for the *all* flow state is closer to the vascular volume fraction of vessel A. In this case, the single-vessel CPD estimates do not superimpose in a straightforward fashion. In contrast, when the flow rate is increased to 6000 μL/h, vessels A–C each produce a plateau longer than 0.5 mm/s and the majority of vessels show a corresponding improvement in the

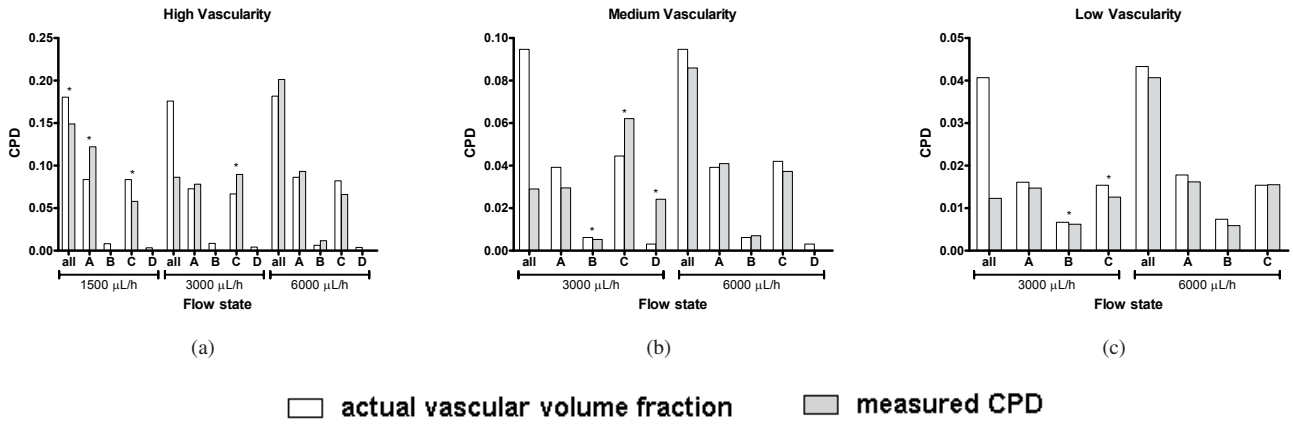

Fig. 4. Comparison between the actual and estimated vascular volume fraction in the flow-phantom experiments for all combinations of flow state and syringe pump flow rate for (a) high, (b) medium, and (c) low vascularity. Asterisks show cases where the length of the plateau was shorter than 0.5 mm/s. A CPD value of zero is shown for cases where no plateau was detected.

accuracy of their measured CPDs compared to their actual vascular volume fractions. As a result, the measured CPD for *all* vessels at 6000 μL/h is closer to the collective vascular volume fraction.

For a multiple-vessel ROI, the first plateau from the left side of the wall-filter selection curve yielded a CPD that was a good estimate of the collective vascular volume fraction when the plateau was longer than 0.5 mm/s and began at a cut-off velocity $<$ 2 mm/s. These conditions were met when the single-vessel wall-filter selection curves consisted of plateaus longer than 0.5 mm/s. When the flow rate in the vascular network was too low to permit these criteria to be met, the multiple-vessel wall-filter selection curve showed a plateau whose CPD corresponded to the vascular volume fraction of a subset of the vessels in the ROI. The reader is referred to [12] for additional details.

The wall-filter selection curve method presented in this paper relies solely on the properties of the ROC curve in an ROI. The applicability to clinical systems, as well as other high-frequency systems, should be straightforward because this technique makes no assumptions about system frequency. For example, Raine-Fenning *et al.* [13] computed a wall-filter selection curve for a 7.5-MHz clinical scanner from a single-vessel ROI and observed a similar shape to the single-vessel selection curves presented in this paper, even with just 5 wall filter cut-offs.

IV. ACKNOWLEDGMENTS

The authors thank Jacques Montreuil, Hristo Nikolov, Joy Dunmore-Buyze, and Mike Bygrave for help with the experimental setup. This research was supported by the Ontario Research and Development Challenge Fund and the University of Western Ontario Schulich School of Medicine and Dentistry. S.Z.P. acknowledges scholarship support from the Natural Sciences and Engineering Research Council of Canada (NSERC PGS-D) and the Ontario Graduate Scholarship Program (OGS).

REFERENCES

[1] J. Folkman, "Angiogenesis: an organizing principle for drug discovery?" *Nature Rev. Drug Discov*, vol. 6, no. 4, pp. 273–286, 2007.

[2] J. R. Less, T. C. Skalak, E. M. Sevick, and R. K. Jain, "Microvascular architecture in a mammary carcinoma: branching patterns and vessel dimensions," *Cancer Res*, vol. 51, no. 1, pp. 265–273, 1991.

[3] R. K. Jain, *Clinical Oncology*, 3rd ed. Philadelphia, PA: Elsevier Churchill Livingstone, 2004, ch. 9.

[4] D. E. Goertz, J. L. Yu, R. S. Kerbel, P. N. Burns, and F. S. Foster, "High-frequency Doppler ultrasound monitors the effects of antivascular therapy on tumor blood flow," *Cancer Res*, vol. 62, no. 22, pp. 6371–6375, 2002.

[5] J. W. Xuan, M. Bygrave, H. Jiang, F. Valiyeva, J. Dunmore-Buyze, D. W. Holdsworth, J. I. Izawa, G. Bauman, M. Moussa, S. F. Winter, N. M. Greenberg, J. L. Chin, M. Drangova, A. Fenster, and J. C. Lacefield, "Functional neoangiogenesis imaging of genetically engineered mouse prostate cancer using three-dimensional power Doppler ultrasound," *Cancer Res*, vol. 67, no. 6, pp. 2830–2839, 2007.

[6] M. Jugold, M. Palmowski, J. Huppert, E. C. Woenne, M. M. Mueller, W. Semmler, and F. Kiessling, "Volumetric high-frequency Doppler ultrasound enables the assessment of early antiangiogenic therapy effects on tumor xenografts in nude mice," *Eur. Radiol*, vol. 18, no. 4, pp. 753–758, 2008.

[7] J. M. Rubin, R. S. Adler, J. B. Fowlkes, S. Spratt, J. E. Pallister, J.-F. Chen, and P. L. Carson, "Fractional moving blood volume: estimation with power Doppler US," *Radiology*, vol. 197, no. 1, pp. 183–190, 1995.

[8] J. M. Rubin, R. O. Bude, J. B. Fowlkes, R. S. Spratt, P. L. Carson, and R. S. Adler, "Normalizing fractional moving blood volume estimates with power Doppler US: defining a stable intravascular point with the cumulative power distribution function," *Radiology*, vol. 205, no. 3, pp. 757–765, 1997.

[9] S. Z. Pinter and J. C. Lacefield, "Detectability of small blood vessels with high-frequency power Doppler and selection of wall filter cut-off velocity for microvascular imaging," *Ultrasound Med. Biol*, 2009, doi:10.1016/j.ultrasmedbio.2009.01.010.

[10] L. K. Ryan and F. S. Foster, "Tissue equivalent vessel phantoms for intravascular ultrasound," *Ultrasound Med. Biol*, vol. 23, no. 2, pp. 261–273, 1997.

[11] K. V. Ramnarine, D. K. Nassiri, P. R. Hoskins, and J. Lubbers, "Validation of a new blood-mimicking fluid for use in Doppler flow test objects," *Ultrasound Med. Biol*, vol. 24, no. 3, pp. 451–459, 1998.

[12] S. Z. Pinter and J. C. Lacefield, "Objective selection of high-frequency power Doppler wall filter cut-off velocity for regions of interest containing multiple small vessels," *IEEE Trans. Med. Imaging*, submitted.

[13] N. J. Raine-Fenning, N. M. Nordin, K. V. Ramnarine, B. K. Campbell, J. S. Clewes, A. Perkins, and I. R. Johnson, "Evaluation of the effect of machine settings on quantitative three-dimensional power Doppler angiography: an *in-vitro* flow phantom experiment," *Ultrasound Obstet. Gynecol*, vol. 32, no. 4, pp. 551–559, 2008.